TOPOLOGICAL OPTICS

Synthesis and observation of non-Abelian gauge fields in real space

Yi Yang[1]*, Chao Peng[2,3], Di Zhu[1], Hrvoje Buljan[4,5], John D. Joannopoulos[1], Bo Zhen[6]*, Marin Soljačić[1]

Particles placed inside an Abelian (commutative) gauge field can acquire different phases when traveling along the same path in opposite directions, as is evident from the Aharonov-Bohm effect. Such behaviors can get significantly enriched for a non-Abelian gauge field, where even the ordering of different paths cannot be switched. So far, real-space realizations of gauge fields have been limited to Abelian ones. We report an experimental synthesis of non-Abelian gauge fields in real space and the observation of the non-Abelian Aharonov-Bohm effect with classical waves and classical fluxes. On the basis of optical mode degeneracy, we break time-reversal symmetry in different manners, via temporal modulation and the Faraday effect, to synthesize tunable non-Abelian gauge fields. The Sagnac interference of two final states, obtained by reversely ordered path integrals, demonstrates the noncommutativity of the gauge fields. Our work introduces real-space building blocks for non-Abelian gauge fields, relevant for classical and quantum exotic topological phenomena.

Gauge fields are the backbone of gauge theories, the earliest example of which is classical electrodynamics. However, until the seminal Aharonov-Bohm effect (*1*), the scalar and vector potentials of electromagnetic fields had been considered as a convenient mathematical aid rather than as objects carrying physical consequences. Berry (*2*) revealed that the Aharonov-Bohm phase imprinted on electrons can be interpreted as a real-space example of geometric phases, which in fact appear in versatile physical systems. For charge-neutral particles, such as photons and cold atoms, synthetic gauge fields can be created in real, momentum, or synthetic (i.e., other parameters besides position or momentum) space. These synthetic gauge fields enable engineered, artificial magnetic fields in systems of either broken or invariant time-reversal symmetry; thus, they play a pivotal role in realizations of topological phases, quantum simulations, and optoelectronic applications.

Gauge fields are classified as Abelian (commutative) or non-Abelian (noncommutative), depending on the commutativity of the underlying group. Synthetic Abelian gauge fields have been realized in various platforms including cold atoms (*3*–*5*), photons (*6*–*8*), polaritons (*9*), and superconducting qubits (*10*). The synthesis of non-Abelian gauge fields is more challenging because of the requirements of degeneracy and noncommutative, matrix-valued gauge potentials. So far, they have been achieved only in momentum and synthetic spaces. Specifically, non-Abelian gauge fields have been realized in momentum space using two-dimensional spin-orbit coupling (*11*, *12*) in cold atoms. In synthetic space, non-Abelian geometric phases (*13*), initially observed in nuclear magnetic resonances (*14*), have enabled non-Abelian geometric gates (*15*) and the simulation of an atomic Yang monopole (*16*).

There have been complementary efforts to synthesize non-Abelian gauge fields in real space. Two initial proposals, using atoms, were based on tripod couplings in spatially varying laser fields (*17*) and laser-assisted, state-dependent tunneling in optical lattices (*18*). Since then, real-space non-Abelian gauge fields have been predicted to enable numerous intriguing phenomena, such as the quantum anomalous Hall effect (*19*), topological insulators in shaken lattices (*20*), and real-space non-Abelian monopoles in superfluids (*21*). To observe non-Abelian gauge fields, Wu and Yang (*22*) conceived the non-Abelian Aharonov-Bohm effect, which has been widely discussed in gauge theory. Moreover, there have been several proposals in atomic (*18*, *23*) and photonic (*24*, *25*) systems that aim at implementing this effect with synthetic gauge fields. Despite

[1]Research Laboratory of Electronics, Massachusetts Institute of Technology, Cambridge, MA 02139, USA. [2]State Key Laboratory of Advanced Optical Communication Systems and Networks, Department of Electronics, Peking University, Beijing 100871, China. [3]Nano-optoelectronics Frontier Center of the Ministry of Education, Beijing 100871, China. [4]Department of Physics, Faculty of Science, University of Zagreb, 10000 Zagreb, Croatia. [5]MOE Key Laboratory of Weak-Light Nonlinear Photonics, TEDA Applied Physics Institute and School of Physics, Nankai University, Tianjin 300457, China. [6]Department of Physics and Astronomy, University of Pennsylvania, Philadelphia, PA 19104, USA. ***Corresponding author. Email: yiy@mit.edu (Y.Y.); bozhen@sas.upenn.edu (B.Z.)**

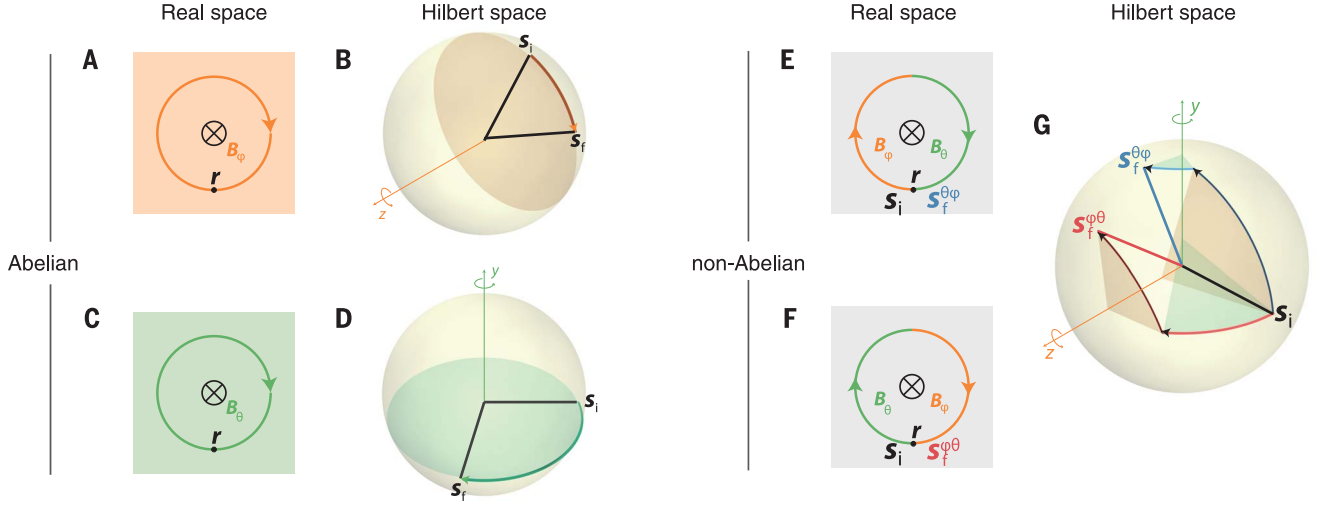

Fig. 1. Comparison between SU(2) Abelian and non-Abelian gauge fields in real space and in Hilbert space. (**A** to **D**) Along a closed loop inside an Abelian gauge field proportional to $\boldsymbol{\sigma}_z$ (A) or $\boldsymbol{\sigma}_y$ (C), the state evolves by rotating around the *z* (B) or *y* (D) axis of the Poincaré sphere. Within each case [(A) and (B), or (C) and (D)], the state evolution is always commutative. (**E** and **F**) In non-Abelian gauge fields, the evolution operators for different loops are no longer commutative, which leads to different final states, $\mathbf{s}_f^{\theta\phi}$ and $\mathbf{s}_f^{\phi\theta}$, for the same initial state $\mathbf{s}_i$. The noncommutativity can be tested by an Aharonov-Bohm interference of the two final states.

these theoretical advances, the synthesis and observation of non-Abelian gauge fields in real space remain experimentally elusive.

We report the observation of the non-Abelian Aharonov-Bohm effect by synthesizing non-Abelian gauge fields in real space. Exploiting a degeneracy in photonic modes, we created non-Abelian gauge fields by cascading multiple nonreciprocal optical elements that break the time-reversal symmetry in orthogonal bases of Hilbert space.

Synthetic non-Abelian gauge fields demand a degeneracy of levels, which can, for example, be achieved by making use of the internal degrees of freedom in quantum gases or exploiting the polarization/mode degeneracy and electromagnetic duality in photons. For a particle moving along a closed path in a non-Abelian gauge field, its evolution operator reads $\mathbf{W} \equiv \mathcal{P} \exp i \oint \mathbf{A}\, \mathbf{dl}$, where $\mathcal{P}$ represents a path-ordered integral and $\mathbf{A}$ is the matrix-valued gauge field. Its trace, $W \equiv \mathrm{Tr}\, \mathbf{W}$, is gauge-invariant and is also known as the Wilson loop. For particles with N-fold degeneracies, the non-Abelian gauge fields can take forms of U(N). Here, we focus on the SU(2) gauge fields, because our photonic system enables the definition of a pseudospin—a two-fold degeneracy in the polarization states. Crucially, we focus on the situations where the involved gauge fields break time-reversal symmetry and state transport becomes nonreciprocal. In what follows, we illustrate the consequence of real-space gauge fields on the pseudospin evolution in Hilbert space [i.e., the Poincaré (or Bloch) sphere].

There is a difference between how a state evolves in Abelian gauge fields and how it evolves in non-Abelian gauge fields (Fig. 1). In a uniform Abelian gauge field proportional to $\boldsymbol{\sigma}_z$, the evolution operator along a closed loop can be simplified as $\mathbf{W} = \exp(i\phi\boldsymbol{\sigma}_z)$, where $\boldsymbol{\sigma}_z$ is the z component of the Pauli matrices and ϕ is the flux of the gauge field through this closed loop (Fig. 1A). Consequently, the state rotates by 2ϕ around the z axis of the Poincaré sphere (*26*) (Fig. 1B). If the state evolves along two consecutive closed loops, the two evolution operators are commutative, which reflects the Abelian nature of this gauge field. Similarly, a homogeneous gauge field proportional to $\boldsymbol{\sigma}_y$ in real space (Fig. 1C) is also Abelian, as the state always evolves around the y axis in the Hilbert space (Fig. 1D).

In contrast, non-Abelian gauge fields require inhomogeneous gauge structures. Figure 1, E and F, illustrates such an example where two different $\boldsymbol{\sigma}_z$ and $\boldsymbol{\sigma}_y$ gauge structures are concatenated into one compounded closed loop. The same initial state $\mathbf{s}_\mathrm{i}$ can now evolve into different final states, $\mathbf{s}_\mathrm{f}^{\theta\phi}$ or $\mathbf{s}_\mathrm{f}^{\phi\theta}$ (Fig. 1G), depending on the different ordering—ϕ and then θ, or alternatively, θ and then ϕ—of the two gauge structures. The interference between the two final states $\mathbf{s}_\mathrm{f}^{\theta\phi}$ and $\mathbf{s}_\mathrm{f}^{\phi\theta}$ is known as the non-Abelian Aharonov-Bohm effect (*27*). This effect, as experimentally demonstrated below, is the most direct manifestation of non-Abelian gauge fields in real space.

In our photonic implementation, we experimentally synthesize the inhomogeneous gauge potentials in a fiber-optic system (Fig. 2A). We identify the horizontal and vertical transverse modes (denoted by $|\mathrm{h}\rangle$ and $|\mathrm{v}\rangle$, respectively) in optical fibers as the pseudospin. Crucially, we synthesize two types of gauge fields, $\phi\boldsymbol{\sigma}_z$ and $\theta\boldsymbol{\sigma}_y$, using two distinct methods to break time-reversal symmetry.

To construct a gauge field of $\phi\boldsymbol{\sigma}_z$, we first use dynamic modulations that dress $|\mathrm{h}\rangle$ and $|\mathrm{v}\rangle$ with nonreciprocal phase shifts of $\pm\phi$, respectively.

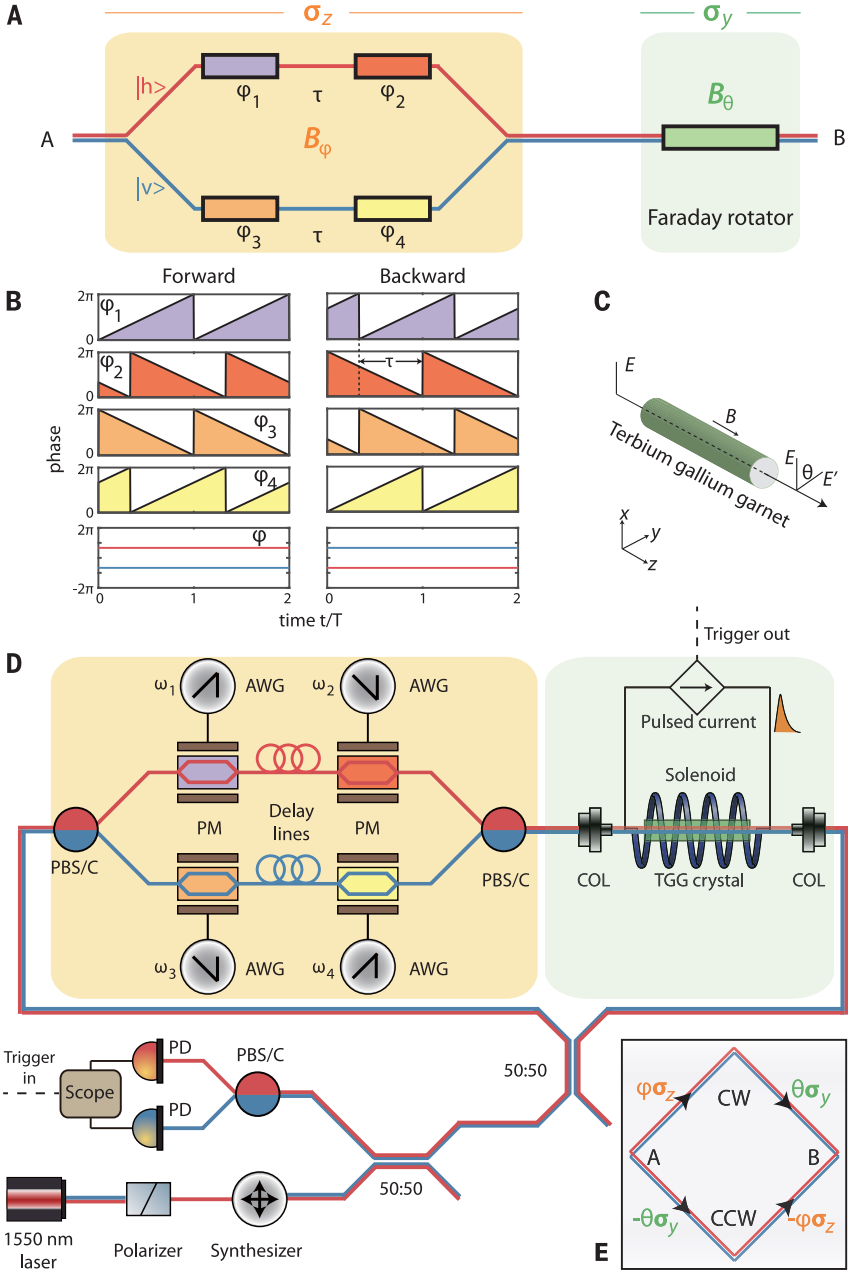

Fig. 2. Synthesis of non-Abelian gauge fields. (**A**) Non-Abelian gauge fields for photons. Temporal modulation and the Faraday effect, which break time-reversal symmetry in two orthogonal bases of the Hilbert space, are used to synthesize $\boldsymbol{\sigma}_z$ and $\boldsymbol{\sigma}_y$ gauge fields, respectively. (**B**) Synthesis of $\boldsymbol{\sigma}_z$ gauge field. Pseudospin-dependent nonreciprocal phase shifts are created through sawtooth phase modulations. (**C**) Synthesis of $\boldsymbol{\sigma}_y$ gauge field. Nonreciprocal rotation of the pseudospin is achieved via the Faraday effect in a terbium gallium garnet crystal. (**D**) Experimental setup. The interference between different final pseudospin states—originating from reversed ordering of the gauge structures—is read out through a Sagnac interferometer, which gives rise to the non-Abelian Aharonov-Bohm effect. PBS/C, polarization beam splitter/combiner; PM, phase modulator; AWG, arbitrary waveform generator; COL, collimator; TGG, terbium gallium garnet; PD, photodetector. (**E**) Schematic of interference between clockwise (CW) and counterclockwise (CCW) pathways.

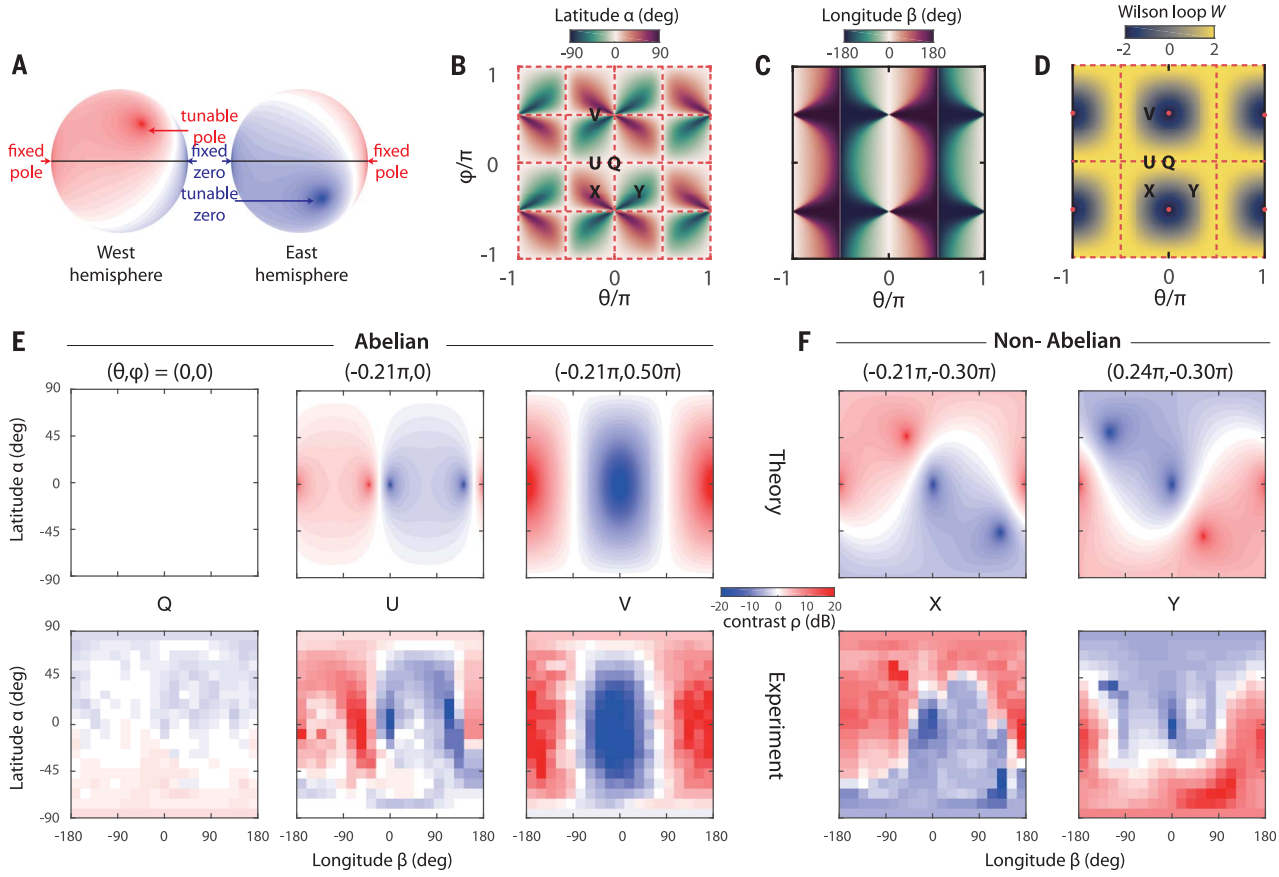

Fig. 3. Non-Abelian Aharonov-Bohm interference. (**A**) Contrast function ρ on the Poincaré sphere, featured by a fixed zero/pole pair (on the equator) and a tunable zero/pole pair (which indicates the consequence of gauge fluxes). The two pairs of zeros and poles are always antipodal. (**B** and **C**) Location (latitude and longitude) of the tunable pole on the Poincaré sphere as a function of the gauge fluxes (θ, ϕ). Abelian gauge fields correspond to on-equator poles (red dashed lines); non-Abelian gauge fields correspond to off-equator poles, both of which are experimentally demonstrated. (**D**) Wilson loops *W* on the synthetic torus (θ, ϕ). |*W*| = 2 (red dashed lines) is a necessary but insufficient condition for non-Abelian gauge fields [compare to (B)]. (**E** and **F**) Examples of predicted and observed contrast functions ρ for Abelian (Q, U, and V) and non-Abelian (X and Y) gauge fields.

Specifically, four lithium niobate phase modulators—two (labeled 1 and 2) for $|h\rangle$ and two (labeled 3 and 4) for $|v\rangle$—are driven by arbitrary waveform generators that create phase shifts in the form of sawtooth functions in time (Fig. 2B). Modulators 1 and 4 are positive in slope, $\phi_{1,4} = \omega t \bmod 2\pi$, whereas modulators 2 and 3 are negative in slope, $\phi_{2,3} = -\omega t \bmod 2\pi$. The delay line between modulators 1 and 2 (3 and 4) corresponds to a delay time τ. As a result, besides dynamic phases, $|h\rangle$ ($|v\rangle$) picks up an extra phase $\phi = \omega\tau$ ($-\omega\tau$) in the forward (i.e., left-to-right) direction, but an opposite phase $-\phi$ ($+\phi$) in the backward direction. This pair of opposite nonreciprocal phases for opposite pseudospin components ($|h\rangle$ and $|v\rangle$) corresponds to a $\phi\boldsymbol{\sigma}_z$ gauge field, which is continuously tunable by varying the modulation frequency ω.

A second, orthogonal type of gauge field, $\theta\boldsymbol{\sigma}_y$, is created using the Faraday effect (Fig. 2C). Specifically, light is coupled out of the fiber, sent through a terbium gallium garnet crystal placed in an external magnetic field, and then coupled back into the fiber. Through the Faraday effect, pseudospin of light is rotated in a nonreciprocal way, which corresponds to a gauge field of $\theta\boldsymbol{\sigma}_y$. This gauge field is also continuously tunable through the external magnetic field.

We then concatenate the two non-Abelian gauge fields to demonstrate the non-Abelian Aharonov-Bohm effect via Sagnac interferometry (Fig. 2, D and E). In such a Sagnac configuration, the two sites A and B in Fig. 2A are combined into the same physical location to enable well-defined non-Abelian gauge fluxes. Evolved from the clockwise (CW) and counterclockwise (CCW) paths of the Sagnac loop, the two final states are $\mathbf{s}_f^{\theta\phi} = \boldsymbol{\sigma}_z \exp(i\theta\boldsymbol{\sigma}_y) \exp(i\phi\boldsymbol{\sigma}_z)\mathbf{s}_i$ and $\mathbf{s}_f^{\phi\theta} = \exp(-i\phi\boldsymbol{\sigma}_z) \exp(-i\theta\boldsymbol{\sigma}_y)\boldsymbol{\sigma}_z\mathbf{s}_i$, where the $\boldsymbol{\sigma}_z$ term maintains a consistent handedness of the polarization for counterpropagating states. The interference of the two final states is given by

$$\mathbf{s}_f = \mathbf{s}_f^{\theta\phi} + \mathbf{s}_f^{\phi\theta} = -\boldsymbol{\sigma}_x[\exp(i\theta'\boldsymbol{\sigma}_y)\exp(i\phi\boldsymbol{\sigma}_z) + \exp(i\phi\boldsymbol{\sigma}_z)\exp(i\theta'\boldsymbol{\sigma}_y)]\mathbf{s}_i \quad (1)$$

(*28*), where $\theta' = \theta + \pi/2$ and $\boldsymbol{\sigma}_x$ is a global spin flip. This interference describes a Sagnac-type realization of the non-Abelian Aharonov-Bohm effect (*27*)—the interference between two final states that originate from the same initial state but undergo reversely ordered, inhomogeneous path integrals (Fig. 1, E and G) in the CW and CCW directions.

In our experimental setup (Fig. 2D) (*28*), we place a polarization synthesizer in front of the Sagnac loop to prepare any desired pseudospin state as the input in a deterministic manner. After exiting the Sagnac loop, the two final states $\mathbf{s}_f^{\theta\phi}$ and $\mathbf{s}_f^{\phi\theta}$ interfere with each other. The associated interference intensity is projected onto the horizontal and vertical bases, which are then measured separately. Within the Sagnac loop, a solenoid—driven by tunable pulsed currents (peak current ≈ 2 kA, duration ≈ 10 ms)—provides a magnetic field between 0 and ~2 T (*28*) for the Faraday rotator. The solenoid also provides a temporal trigger signal for the detection. For the dynamic modulation, we assign four different modulation frequencies (i.e., slopes of the temporal sawtooth functions) $+\omega_1$, $-\omega_2$, $-\omega_3$, and $+\omega_4$ to each of the modulators with ω_j (j = 1, 2, 3, 4) defined to be positive. We impose

an additional constraint that $\omega \equiv (\omega_1 + \omega_2)/2 = (\omega_3 + \omega_4)/2$. This modified arrangement from Fig. 2B maintains the same nonreciprocal phases and thus the gauge fields $\phi\boldsymbol{\sigma}_z$ (*28*). The advantage of this modification is an experimental one: It relocates the relevant interference fringes from zero to a nonzero carrier frequency $\Omega \equiv \omega_1 - \omega_2 + \omega_3 - \omega_4$, which is less sensitive to environmental or backscattering noises.

We next define our experimental observable and explain its relevance to non-Abelian gauge fields. In the original U(1) Abelian Aharonov-Bohm effect, the observable is the interference intensity as a function of the Abelian magnetic flux. In our case, analogously, for each given set of non-Abelian gauge fields (θ, ϕ), we measure the contrast ρ between the interference intensities projected onto the horizontal and vertical bases. Specifically, we measure $\rho(\theta, \phi, \alpha, \beta) \equiv I_{\mathrm{h}}^{\Omega}/I_{\mathrm{v}}^{\Omega}$, where (α, β) are the latitude and longitude of the input pseudospin state on the Poincaré sphere and $I_{\mathrm{h(v)}}^{\Omega}$ are the intensities of the $|\mathrm{h}\rangle$ and $|\mathrm{v}\rangle$ components of the output pseudospin state at the carrier frequency Ω, respectively. Therefore, ρ is defined on a manifold of $S^2 \times T^2$, which is spanned by the Hilbert space of the input pseudospin S^2 and the synthetic space of the gauge fields (θ, ϕ) that is T^2.

For a fixed set of gauge fields (θ, ϕ), the contrast function $\rho(\alpha, \beta)$ always exhibits two pairs of first-order zeros and poles on the Poincaré sphere (Fig. 3A) (*28*). Within each pair, the zero and the pole are always antipodal and thus represent orthogonal pseudospins. One pair, being linear polarizations (1, 0) (zero) and (0, 1) (pole), is fixed on the two ends of the equator, regardless of the choice of (θ, ϕ). The other orthogonal pseudospin pair, however, is tunable on the entire sphere via (θ, ϕ). These zeros and poles are conserved quantities on the Poincaré sphere and dictate the behavior of the contrast ρ function. Their generation, evolution, and annihilation are directly related to the transitions between the Abelian and non-Abelian regimes. Figure 3, B and C, shows the latitude α and longitude β of the tunable pole on the Poincaré sphere as a function of gauge fields (θ, ϕ). When $\theta = m\pi/2$ or $\phi = n\pi/2$ (m and n are integers), the tunable zero-pole pair appears on the equator (red dashed lines in Fig. 3B). This key feature—an on/off-equator zero/pole—can be used to straightforwardly differentiate between Abelian and non-Abelian gauge fields synthesized in our experiment (Fig. 3, E and F).

The necessary and sufficient condition for gauge fields to be non-Abelian is as follows. There exist two loop operators, $\mathbf{W}_1$ and $\mathbf{W}_2$, both starting and ending at the same site in space, such that they are noncommutative; that is, $\mathbf{W}_1\mathbf{W}_2 \neq \mathbf{W}_2\mathbf{W}_1$ (*29*). In an Aharonov-Bohm interference, whether Abelian or non-Abelian, $\mathbf{W}_1$ and $\mathbf{W}_2$ can be identified as a pair of time-reversal partners that share the same physical path. We first examine $\mathbf{W}_1 = l_{\mathrm{b}}^{-1} \cdot l_{\mathrm{t}}$ and $\mathbf{W}_2 = l_{\mathrm{t}}^{-1} \cdot l_{\mathrm{b}}$ in the Abelian Aharonov-Bohm experiment, whose two distinct top and bottom paths are denoted by l_{t} and l_{b}, respectively. Under time reversal, both momentum and vector potentials flip sign, rendering $\mathbf{W}_1 = \mathbf{W}_2 = \exp(i\gamma)$. $\mathbf{W}_1$ and $\mathbf{W}_2$ are clearly commutative and exhibit identical, scalar Berry phases γ (*28*). In our non-Abelian Aharonov-Bohm experiment, the time-reversal pair $\mathbf{W}_1$ and $\mathbf{W}_2$ can be analogously defined by replacing l_{t} and l_{b} with CW and CCW paths (Fig. 2E), which yields

$$\mathbf{W}_1 = \mathcal{P}\exp i \oint_{\mathrm{CCW}^{-1}\cdot\mathrm{CW}} \mathbf{A}\,\mathrm{d}\mathbf{l}$$

$$= \boldsymbol{\sigma}_z[\exp(i\theta\boldsymbol{\sigma}_y)\exp(i\phi\boldsymbol{\sigma}_z)]\boldsymbol{\sigma}_z[\exp(i\theta\boldsymbol{\sigma}_y)\exp(i\phi\boldsymbol{\sigma}_z)] \quad (2)$$

$$\mathbf{W}_2 = \mathcal{P}\exp i \oint_{\mathrm{CW}^{-1}\cdot\mathrm{CCW}} -\mathbf{A}\,\mathrm{d}\mathbf{l}$$

$$= [\exp(i\phi\boldsymbol{\sigma}_z)\exp(i\theta\boldsymbol{\sigma}_y)]\boldsymbol{\sigma}_z[\exp(i\phi\boldsymbol{\sigma}_z)\exp(i\theta\boldsymbol{\sigma}_y)]\boldsymbol{\sigma}_z \quad (3)$$

(*28*). The condition for $\mathbf{W}_1$ and $\mathbf{W}_2$ to be noncommutative is satisfied when $\theta \neq m\pi/2$ and $\phi \neq n\pi/2$ (*28*); the same condition also guarantees the existence of a zero and a pole of the contrast function away from the equator (Fig. 3B). Because $\mathbf{W}_1$ and $\mathbf{W}_2$ are also connected via a unitary gauge transformation (*28*), they always share the same Wilson loop (*28*): $W = \mathrm{Tr}\,\mathbf{W}_1 = \mathrm{Tr}\,\mathbf{W}_2 = 2 - (4\cos^2\theta\sin^2\phi)$. Figure 3D shows this Wilson loop on the T^2 space of gauge fields. Generally speaking, in an N-fold degenerate system, $|W| = N$ means that the state evolution can be trivially understood by decoupling the system into the product of N Abelian subsystems (*29*). In our case, such trivial configurations are shown with red dashed lines [$\theta = (m + {}^1/_2)\pi$; $\phi = n\pi$; or $\theta = m\pi$ and $\phi = (n + {}^1/_2)\pi$] in Fig. 3D. Nonetheless, $|W| \neq N$ is only a necessary but insufficient condition for gauge fields to be non-Abelian (*29*), as is evident from the comparison between Fig. 3B and Fig. 3D: Some configurations with $|W| \neq N$ are still Abelian. This is supported by recent observations from photonic waveguides, where non-Abelian geometric phases can arise from Abelian gauge fields (*30*).

We then characterize our synthetic gauge fields by measuring the contrast function ρ (Fig. 3, E and F). A comparison is made between theoretical predictions (top row) and experimental measurements (bottom row) for five sampling points on the synthetic space T^2: Q, U, and V are Abelian, and X and Y are non-Abelian. In the Abelian case Q [$(\theta, \phi) \approx (0, 0)$], the tunable pole and the fixed zero annihilate each other at $(\alpha, \beta) = (0°, 0°)$; so do the tunable zero and the fixed pole at $(\alpha, \beta) = (0°, 180°)$. As a result, the contrast remains a constant $\rho = 1$ regardless of the input pseudospin state. This is a direct consequence of the preserved time-reversal symmetry in the absence of gauge fluxes. In case U [$(\theta, \phi) \approx (-0.21\pi, 0)$], the annihilation of poles with zeros is lifted; nonetheless, both poles and zeros appear on the equator, and the gauge structure remains Abelian, because we only break time-reversal symmetry once. In case V [$(\theta, \phi) \approx (-0.21\pi, 0.50\pi)$], which is still Abelian, the two poles (zeros) coalesce and produce a second-order pole (zero) on the equator. In cases X [$(\theta, \phi) \approx (-0.21\pi, -0.30\pi)$] and Y [$(\theta, \phi) \approx (0.24\pi, -0.30\pi)$], the synthetic gauge fields become non-Abelian, as indicated by the observed off-equator zeros and poles. For all the cases, our observations show agreement with the associated predictions. In our interferometer, the two spin bases $|\mathrm{h}\rangle$ and $|\mathrm{v}\rangle$ are not perfectly degenerate because of the difference in their refractive indices ($\sim 10^{-4}$). This difference leads to a reciprocal, linear birefringent phase (i.e., a dynamic phase contribution), which is calibrated and consistently applied to all measurements (*28*).

Up to this point, we have measured the contrast ρ for fixed gauge fluxes while changing the input states. In a complementary manner, we can now fix the input state (α, β) and demonstrate the tunability of the synthesized non-Abelian gauge fields by measuring the contrast ρ for different synthetic gauge fluxes (θ, ϕ). As shown in Fig. 4, we reach similar agreement between the theoretical prediction and the measurement.

We have demonstrated an experimental synthesis of non-Abelian gauge fields in real space, which is confirmed by our observation of the non-Abelian Aharonov-Bohm effect using classical particles and classical fluxes. The realized gauge fields demonstrate a viable way to engineer

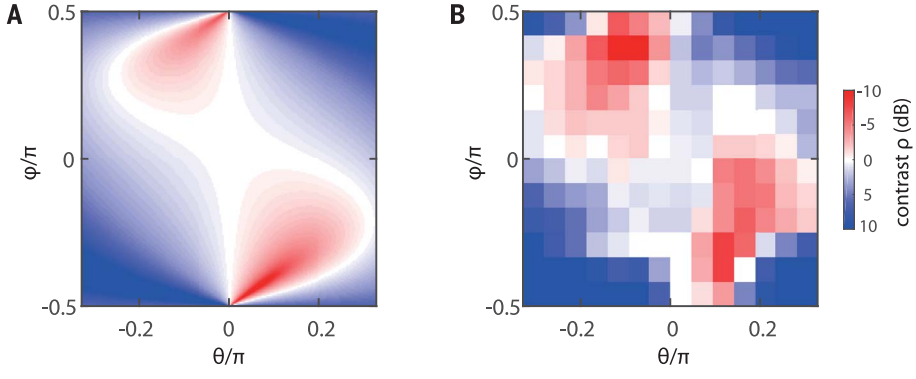

Fig. 4. Tunability of the non-Abelian gauge fields. (**A** and **B**) Predicted (A) and measured (B) contrast function ρ for a fixed incident pseudospin state $(\alpha, \beta) \approx (-51°, -12°)$. The gauge fields $\phi\boldsymbol{\sigma}_z$ and $\theta\boldsymbol{\sigma}_y$ are continuously tuned by respectively varying the modulation frequencies in the arbitrary waveform generators and the voltages applied to the solenoid.

the Peierls phase in the simulation of topological systems, such as the non-Abelian Hofstadter models (*18*) [see also our lattice models (*28*)]. Our experiment also introduces non-Abelian ingredients for realizing high-order topological phases and topological pumps. In addition, recent advances in on-chip modulation and magneto-optical materials could enable future observations of non-Abelian topology in integrated photonic platforms. Toward the quantum regime, non-Abelian gauge fields might be used to help generate non-Abelian anyonic excitation to offer an alternative, synthetic approach for topological quantum computation. Finally, the synergy of non-Abelian gauge fields with engineered interactions (e.g., bosonic blockade and superconducting qubits) might enable the realization of many-body physics such as the non-Abelian fractional quantum Hall effect.

REFERENCES AND NOTES

1. Y. Aharonov, D. Bohm, *Phys. Rev.* **115**, 485–491 (1959).
2. M. V. Berry, *Proc. R. Soc. London Ser. A* **392**, 45–57 (1984).
3. Y.-J. Lin, R. L. Compton, K. Jiménez-García, J. V. Porto, I. B. Spielman, *Nature* **462**, 628–632 (2009).
4. M. Aidelsburger *et al*., *Phys. Rev. Lett.* **107**, 255301 (2011).
5. J. Struck *et al*., *Phys. Rev. Lett.* **108**, 225304 (2012).
6. K. Fang, Z. Yu, S. Fan, *Nat. Photonics* **6**, 782–787 (2012).
7. R. Umucalılar, I. Carusotto, *Phys. Rev. A* **84**, 043804 (2011).
8. L. D. Tzuang, K. Fang, P. Nussenzveig, S. Fan, M. Lipson, *Nat. Photonics* **8**, 701–705 (2014).
9. H.-T. Lim, E. Togan, M. Kroner, J. Miguel-Sanchez, A. Imamoğlu, *Nat. Commun.* **8**, 14540 (2017).
10. P. Roushan *et al*., *Nat. Phys.* **13**, 146–151 (2017).
11. L. Huang *et al*., *Nat. Phys.* **12**, 540–544 (2016).
12. Z. Wu *et al*., *Science* **354**, 83–88 (2016).
13. F. Wilczek, A. Zee, *Phys. Rev. Lett.* **52**, 2111–2114 (1984).
14. J. W. Zwanziger, M. Koenig, A. Pines, *Phys. Rev. A* **42**, 3107–3110 (1990).
15. A. A. Abdumalikov Jr. *et al*., *Nature* **496**, 482–485 (2013).
16. S. Sugawa, F. Salces-Carcoba, A. R. Perry, Y. Yue, I. B. Spielman, *Science* **360**, 1429–1434 (2018).
17. J. Ruseckas, G. Juzeliūnas, P. Öhberg, M. Fleischhauer, *Phys. Rev. Lett.* **95**, 010404 (2005).
18. K. Osterloh, M. Baig, L. Santos, P. Zoller, M. Lewenstein, *Phys. Rev. Lett.* **95**, 010403 (2005).
19. N. Goldman *et al*., *Phys. Rev. Lett.* **103**, 035301 (2009).
20. P. Hauke *et al*., *Phys. Rev. Lett.* **109**, 145301 (2012).
21. E. Yakaboylu, A. Deuchert, M. Lemeshko, *Phys. Rev. Lett.* **119**, 235301 (2017).
22. T. T. Wu, C. N. Yang, *Phys. Rev. D* **12**, 3845–3857 (1975).
23. A. Jacob, P. Öhberg, G. Juzeliūnas, L. Santos, *Appl. Phys. B* **89**, 439–445 (2007).
24. T. Iadecola, T. Schuster, C. Chamon, *Phys. Rev. Lett.* **117**, 073901 (2016).
25. Y. Chen *et al*., *Nat. Commun.* **10**, 3125 (2019).
26. M. A. Nielsen, I. L. Chuang, *Quantum Computation and Quantum Information* (Cambridge Univ. Press, 2010).
27. J. Dalibard, F. Gerbier, G. Juzeliūnas, P. Öhberg, *Rev. Mod. Phys.* **83**, 1523–1543 (2011).
28. See supplementary materials.
29. N. Goldman, G. Juzeliūnas, P. Öhberg, I. B. Spielman, *Rep. Prog. Phys.* **77**, 126401 (2014).
30. M. Kremer, L. Teuber, A. Szameit, S. Scheel, arXiv 1902.02559 [physics.optics] (7 February 2019).

ACKNOWLEDGMENTS

We thank Y. Lin, R. Luo, and S. Yang for assistance in the setup and measurement; C. Chen and F. N. C. Wong for sharing equipment; K. Berggren, D. Englund, L. Fu, M. Kjaergaard, J. Li, E. J. Mele, W. D. Oliver, R.-J. Shiue, and A. Vishwanath for fruitful discussions; and P. Rebusco and J. Sloan for reading and editing of the manuscript. **Funding:** Supported by the Army Research Office under Cooperative Agreement W911NF-18-2-0048, NSF grant CCF-1640012, AFRL contract FA8650-16-D-5403, and the MRSEC Program of NSF under award DMR-1419807; National Natural Science Foundation of China grant 61575002 (C.P.); a National Science Scholarship from A*STAR, Singapore (D.Z.); the QuantiXLie Centre of Excellence, funded by the European Regional Development Fund (grant KK.01.1.1.01.0004) and Croatian Science Foundation grant IP-2016-06-5885 SynthMagIA (H.B.); and the Charles E. Kaufman Foundation, a supporting organization of the Pittsburgh Foundation, and NSF grant DMR-1838412 (B.Z.). **Author contributions:** Y.Y., B.Z., and M.S. conceived and designed the experiment. Y.Y. and C.P. built the setup. Y.Y., C.P., and D.Z. performed the experiment. Y.Y. and B.Z. developed the theory. Y.Y. and B.Z. wrote the manuscript with inputs from all authors. J.D.J., B.Z., and M.S. supervised the research. **Competing interests:** The authors declare no competing interests. **Data and materials availability:** All data needed to evaluate the conclusions in the paper are present in the paper or the supplementary materials.

SUPPLEMENTARY MATERIALS

science.sciencemag.org/content/365/6457/1021/suppl/DC1
Materials and Methods
Figs. S1 to S8
References (*31*–*39*)

7 June 2019; accepted 12 August 2019
10.1126/science.aay3183

Synthesis and observation of non-Abelian gauge fields in real space

Yi Yang, Chao Peng, Di Zhu, Hrvoje Buljan, John D. Joannopoulos, Bo Zhen and Marin Soljacic

Science **365** (6457), 1021-1025.
DOI: 10.1126/science.aay3183

An optical contortionist

The development of gauge fields is fundamental to our theoretical understanding of interactions in physical systems. There are two kinds of fields: Abelian, in which the measured effects on an observable parameter are commutative; and non-Abelian (noncommutative), where the sequence in which the field is applied matters. The latter are more difficult to realize in solid-state systems, but recent theoretical work has suggested that these could be synthesized optically. Yang *et al.* generated non-Abelian gauge fields by cascading multiple nonreciprocal optical elements and verified this accomplishment by the observed interference patterns in a Sagnac interferometer. Having a system that is tunable between Abelian and non-Abelian regimes will be important for studying complex topological states in photonic platforms.

Science, this issue p. 1021